Optical characterization of a low f-number cryogenic spot scan objective for infrared detectors

Joris Goree, Edouard Huard de Verneuil, Julien Jaeck, Olivier Gravrand, Olivier Boulade, Jérome Primot, Sophie Derelle

Optical characterization of a low f-number cryogenic spot scan objective for infrared detectors

Gorée J. Author[a], Huard de Verneuil E.[a], Jaeck J.[a], Gravrand O.[b], Boulade O.[c], Primot J.[a], and Derelle S.[a]

[a]Université Paris-Saclay, ONERA, Optique et techniques associées, 91123, Palaiseau, France
[b]CEA-LETI, Commissariat à l'Énergie Atomique et aux énergies alternatives - Laboratoire d'Électronique et de Technologie de l'Information, 38054 Grenoble, France
[c]CEA-IRFU, Commissariat à l'Énergie Atomique et aux énergies alternatives - Institut de la Recherche sur les lois Fondamentales de l'Univers, 91191 Gif-sur-Yvette, France

ABSTRACT

Infrared focal plane arrays are widely used for astronomical observations and are constantly optimized to provide higher-quality images. The knowledge of the pixel spatial response becomes critical to extract ever more data from scientific missions. A specific cryogenic spot scan objective with an f-number of 1.2 has been developed in order to finely characterize 15 µm (or smaller) pixel pitch cooled infrared focal plane arrays in the spectral band between 3-5 µm. It will be operated in the MIRCOS test bench with different narrow-band filters. We present the first optical characterization of this objective obtained with a cryogenic wavefront analyzer – a quadrilateral shearing interferometer. The measured wavefront indicates a peak-to-valley amplitude of 2 µm, which corresponds to an optical quality of about $\lambda/2$ at 3.75 µm working wavelength. This value higher than expected might be due to a non-uniform cooling of the objective.

Keywords: Infrared, Cryogenics, Spot scan, Wavefront

1. INTRODUCTION

The quest for celestial bodies by the astrophysics community results in an increased need for high spatial or spectral resolution imaging. As a result, technology is evolving to meet these critical needs. In the infrared domain, the format of quantum Focal Plane Array (FPA) is increasing and generally leads to a reduction of the pixel size. Indeed, the size of the pixel has been decreasing continuously during the last 20 years, going from 30µm to 15µm,[1,2] 12µm,[3] 10µm[4] or even 5µm.[5] These evolutions make it more difficult to precisely know the spatial response of the pixel through the Modulation Transfer Function (MTF) and/or the Point Spread Function (PSF). However, the measurement of the PSF/MTF is essential for manufacturers in order to optimize detection structures and for scientists in the development and operation of instruments. As a result, current characterization methods must be adapted to accurately measure these figures of merit that reflect the FPA's ability to spatially reproduce fine details of the scene.

The key point of measuring small infrared pixel spatial response is to project a fine and well-known spot onto the FPA. To reach this goal, several methods have been developed in the community:

- The most used method consists of the optical characterization of the spot scan objective with a small diode: the shape of the projected optical PSF is measured by scanning a tiny diode over the spot.[6] This method is straightforward but can become difficult as the diode becomes wavelength sized.

Further author information:
Gorée J.: E-mail: joris.goree@onera.fr

- A second method imagined by the manufacturer SemiConductor Devices (SCD) consists in uniformly illuminating the back of the FPA, covered with a thin layer of gold on which square apertures of 4 µm side have been located at precise positions in relation to the array.[7] This method allows reconstituting a spot scan-like measurement without scanning nor imaging optics, assuming that all pixels are identical. However, the issue of the diffraction induced by the sub-wavelength apertures is not taken into account and can have a serious impact on the final result.
- A third method uses a diffraction-limited spot scan objective operating at shorter wavelengths.[8] In this case, the spot size remains small even with a higher optical F-number, which makes it easier to carry out the measurement. However, the pixel spatial response is not measured in the spectral band of interest, and it is not possible to study the potential impact of the wavelength on the PSF.

All those methods also have to deal with the restrictions resulting from a high thermal background in the Infrared (IR) spectrum. Indeed, access to the FPA is restricted due to the size of the dewar and the presence of the cold shield surrounding it to limit the thermal background and increase the signal-to-noise ratio. In this case, the fineness of the final projected pattern can be reduced because it is directly related to the opening of the cold shield.

The method presented in this paper uses a high-quality spot scan mid-infrared objective in a controlled and low background environment inside the "Moyen Infrarouge Refroidi pour la Caractérisation d'Optiques et de Systèmes" (MIRCOS) bench. An absolute optical characterization of the objective by a wavefront FPA is part of the spot deconvolution procedure.

2. DESCRIPTION OF THE SPOT SCAN BENCH

The MIRCOS bench, developed in 2018 at ONERA, is a versatile cryogenic test platform that can accommodate a cryogenic projection system (grating, spot scan objective, etc.) mounted on a set of nanometer linear stages in the same cold shield as the FPA. Such a system allows the projection of the finest possible patterns while limiting the stray thermal radiation, which improves the signal-to-noise ratio. Fig.1 and Fig.2 show the drawing and pictures of the measurement bench. As shown in Fig. 1, a collimated light beam from a black body heated at 1473K is focused by the condenser on the object pinhole. Next, the spot scan objective images the object hole onto the FPA, which has its own dewar as shown in Fig. 2a.

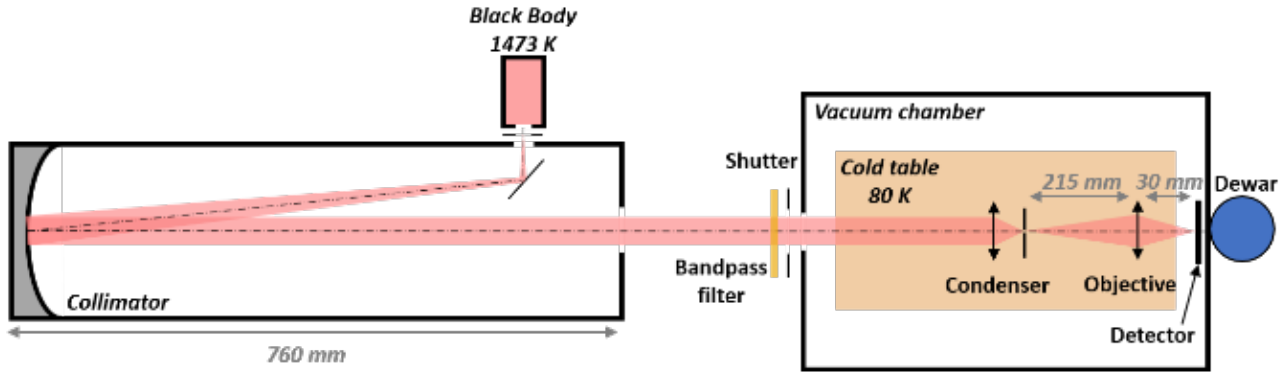

Figure 1: Drawing of the PSF measurement bench

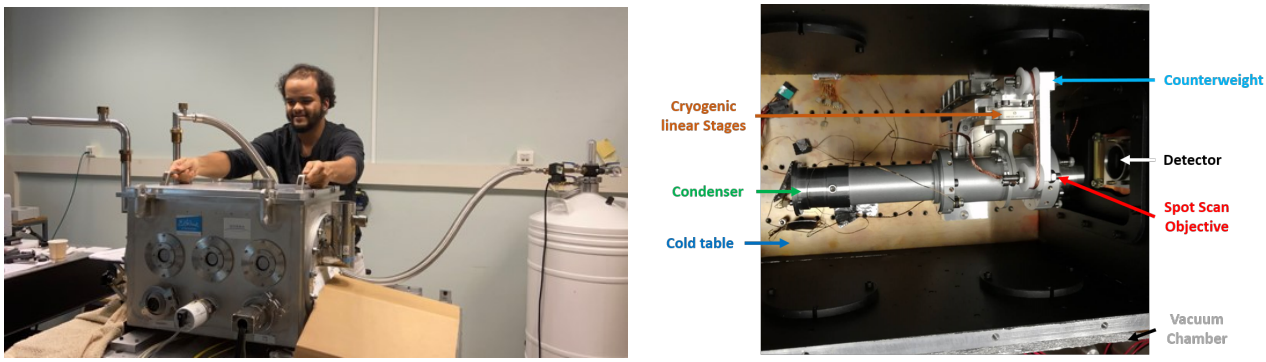

(a) Picture of the outside of the MIRCOS bench.

(b) Zoom of the inside of the vacuum chamber.

Figure 2: Pictures of the PSF measurement bench

This bench has been used previously to study the MTF on a HgCdTe Mid-Wave Infrared (MWIR) FPA using a 2D interferometric method developed at ONERA. In this paper, the projection system used to measure the PSF of a FPA is an objective designed and manufactured by Winlight System. It works in the MWIR range ($3 - 5.5$ µm) and has a focal length of 25 mm. With an F-number equal to 1.2, it has been designed to work in a finite-finite configuration at 80K.

2.1 MIRCOS cryogenic chamber

An illustration and a picture of the bench are presented in Fig.2b and Fig.1. The light beam comes from a blackbody heated at 1473K, which illuminates a hole placed at the focal point of the collimator. Then, the collimated beam goes through a 60 mm diameter Z_nS_e window of the vacuum chamber (10^{-6} bar) and enters into the cryogenic chamber cooled at 80K. A narrow bandpass filter can be added in front of the window in order to limit the blackbody spectral band. Cooling is achieved by pouring liquid nitrogen into the cold table, and the final temperature is generally reached in approximately 5h. The temperature is maintained at 80K by using an electrovalve (placed on a self-pressurized liquid nitrogen dewar) monitored by two temperature probes. Additional probes provide real-time temperature monitoring on different components (projection system, cold shield...) inside the cryogenic chamber. The advantage of MIRCOS is that different systems can be integrated into the same cold shield as the FPA, allowing a low F-number. For this purpose, the vacuum chamber is 56 *cmr* long, 39 cm large and 40 cm high while the cold shield is 42 cm long, 17 cm large and 20 cm high.

2.2 Cryogenic spot scan objective

The spot scan technique is based on a 2D displacement of the cryogenic objective in order to scan along two perpendicular axes of the FPA. Indeed, a light spot is locally projected onto the FPA. Then, a 2D scan is operated using the cryogenic linear stages. During this measurement, the response of a given pixel is acquired in order to obtain the spatial response of the pixel after the deconvolution is performed. The principle of the spot scan technique is shown in Fig. 3.

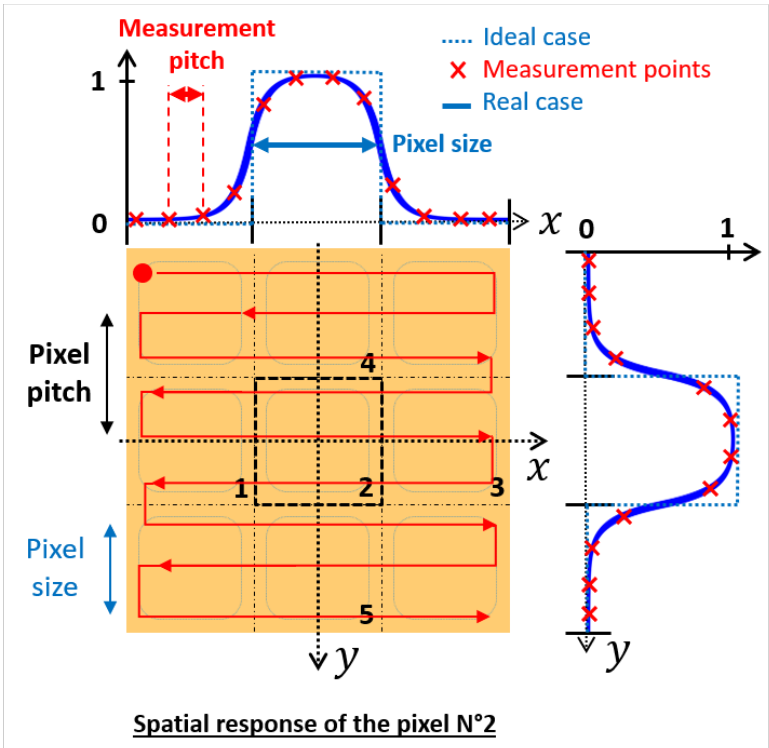

Figure 3: Principle of the spot scan technique.

Deconvolution can only be achieved with knowledge of the optical spatial response of the cryogenic objective, as shown in Eq. 1:

$$PSF_{Measured} = PSF_{Pixel} * PSF_{Objective} \tag{1}$$

The projection system used to measure the PSF of the FPA is an objective designed and manufactured by Winlight System, as it is shown in Fig.2b. It operates in the MWIR band ($3 - 5.5\mu m$) and has a focal length of 25 mm. The F-number is equal to 1.2. It has been designed to operate in a finite-to-finite configuration at a working temperature of 80K. This configuration is achieved by placing a 15 µm diameter pinhole object at a distance of 215 mm from the principal object plane of the objective so that the magnification equals 1/3. A condenser focuses the collimated incoming light on the pinhole, increasing the signal-to-noise ratio. The pinhole and the condenser are mechanically bound to the objective.

This overall setup has two advantages: it allows a precise centering of the pinhole with the objective in order to minimize off-axis aberrations. The geometric image is also equivalent to the Full Width at Half Maximum (FWHM) of the objective Airy spot (which is about 4.9 µm at 4 µm of wavelength). Even if the theoretical FWHM is relatively small, it is not negligible compared to 15 µm or smaller pixel pitches. A fine optical characterization of the objective is then needed to perform an accurate deconvolution on the measured PSF and get the pixel PSF.

2.3 Cryogenic linear stages

In order to scan the spot on the FPA along three translation axes, cryogenic linear stages (manufactured by Attocube) are installed inside the cold shield. Those stages have an entire course of 20 mm, which covers the whole surface of the FPA. However, the vertical stage tolerates a maximum weight of 200 g, which roughly corresponds to the spot scan objective's weight. Therefore, we chose to use a counterweight to lighten the load

on the vertical stage and thus allow the system to move correctly. The counterweight connected to the objective via a copper braid and two Teflon pulleys can be seen in Fig. 5d.

The cryogenic stages are equipped with resistive encoders to control their position. However, the reading accuracy of these encoders is only about 1 to 2 µm, which is insufficient to move the stages very precisely for characterizing small pixels of at most 10 µm. Indeed, the required accuracy is the order of 100 nm. Interferometric sensors (manufactured by Attocube) have then been added to each linear stage to address this issue. Their technology is based on a Fabry-Perot interferometer. The wavelength for the measurement laser is at 1.53 µm. The composition of the FPA is shown in Fig. 4: An optical fiber that guides the wave is plugged into the FPA head. Then, a retroreflector, a corner-cube mirror, reflects the wave to the FPA head and lets it make its way back and interfere.

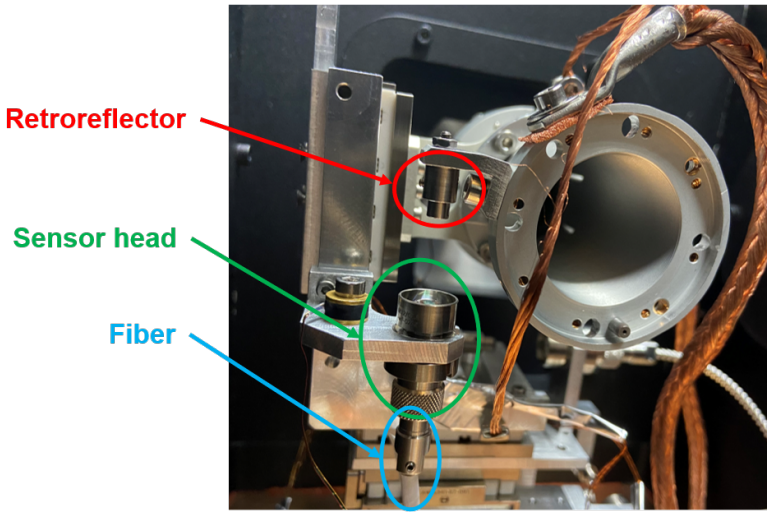

Figure 4: Picture of the interferometric sensor.

Such FPAs can be used in vacuum and cryogenic conditions while being very accurate (accuracy in the nanometer range). They are also usually used in a closed-loop to position the stages. In addition to being compact and modular, the advantages of this system are the working distance which can be up to several meters depending on which FPA head is used. Since the displacement range of the stages is 20 mm and the desired accuracy is at most 100 nm (for a 10 µm pixel size), the interferometric sensors perfectly meet the requirements.

2.4 Embedding of the FPA

We noticed that, without moving the stages, the position of the spot on the FPA was variable over time. More specifically, the position of the spot changed according to the liquid nitrogen filling in the FPA Dewar. Indeed, the variation of the volume of liquid nitrogen in the Dewar creates a mechanical or thermal effect on the cold table of the FPA, causing it to move. The best way to prevent the FPA from moving because of thermal effects is to remove the dewar. Therefore, a custom cold table and specific tooling were manufactured to mount the FPA directly on the cold shield of the MIRCOS bench.

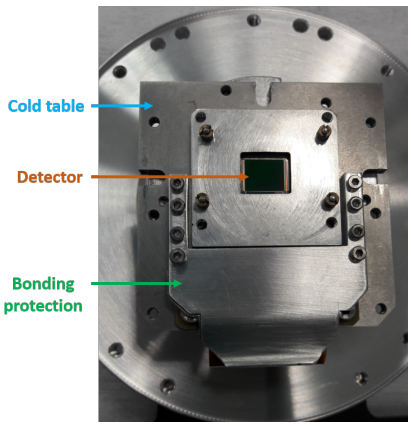

(a) FPA on its cold table.

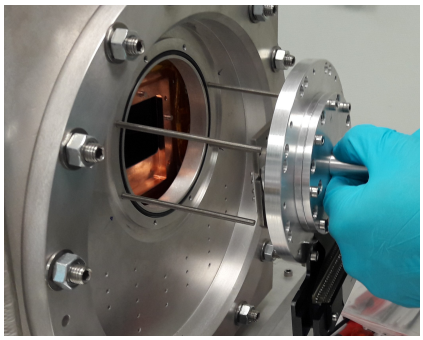

(b) Rear view (Implementation of the FPA).

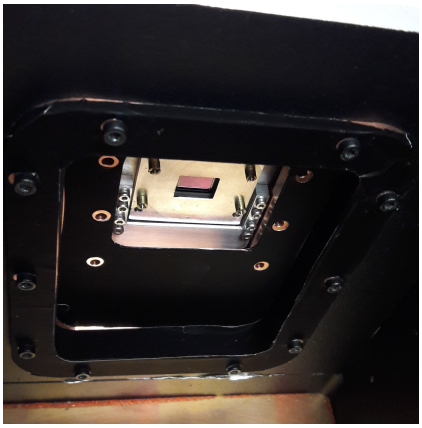

(c) Front view inside the MIRCOS platform.

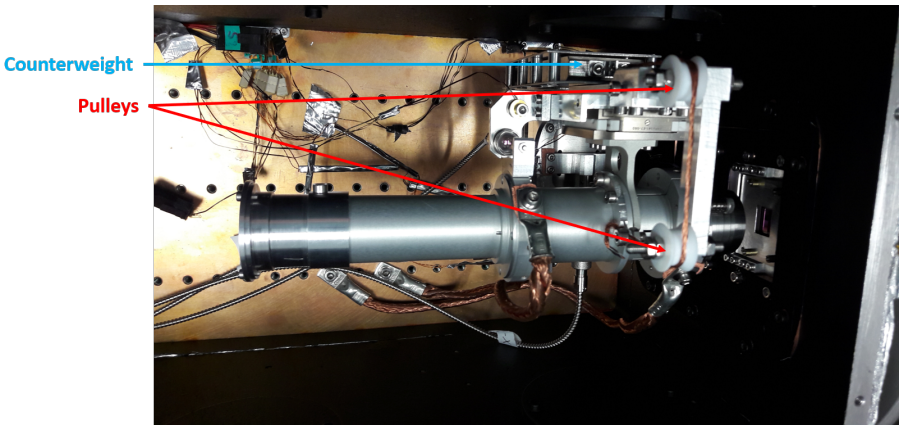

(d) Optical bench inside the MIRCOS platform.

Figure 5: Views of the assembly for embedding the FPA inside MIRCOS

As shown in Fig. 5c, the front of the parts assembly has a black coating to avoid stray reflections. The cooling of the FPA is ensured by the cold table, which is attached behind the FPA, as shown in Fig. 5a. Fig. 5b shows the process of installing the FPA inside the cold shield using an extractor.

3. OPTICAL CHARACTERIZATION OF THE OBJECTIVE

Deconvolution of the measurement of the spatial response of the pixel requires a perfect knowledge of the optical PSF of the objective. We use a wavefront analyzer to achieve this goal. It will then be possible to estimate the optical PSF from the wavefront measurement.

3.1 Working principle of the wavefront analyzer

The analyzer is based on a Quadri-Lateral Shearing Interferometer (QLSI). This interferometer is based on a particular continuously self-imaging grating named Modified Hartmann Mask (MHM)[9,10] coupled with a FPA. The MHM looks like a chessboard where the hole-period ratio is specifically chosen to mainly diffract four orders which are slightly tilted.[11] The interference pattern is located where the four replicas overlap.[12] The intensity of this interference pattern depends on the input wavefront W and is given by Eq. 2[13] :

$$I_z(x,y) = \frac{I_0}{16}\left\{ \begin{array}{l} 4 + 4\cos\left[\frac{2\pi x}{p} + \frac{2\pi z}{p}\frac{\partial W}{\partial x}(x,y)\right] + 4\cos\left[\frac{2\pi y}{p} + \frac{2\pi z}{p}\frac{\partial W}{\partial y}(x,y)\right] + \\ 2\cos\left[\frac{2\sqrt{2}\pi x'}{p} + \frac{2\sqrt{2}\pi z}{p}\frac{\partial W}{\partial x'}(x,y)\right] + 2\cos\left[\frac{2\sqrt{2}\pi y'}{p} + \frac{2\sqrt{2}\pi z}{p}\frac{\partial W}{\partial y'}(x,y)\right] \end{array} \right\} \quad (2)$$

where p is the period of the interferogram along x-axis or y-axis and is equal to the half of the period of the grating. z is the observation distance from the grating. Coordinates (x', y') are given by: $x' = (x-y)/\sqrt{2}$ and $y' = (x+y)/\sqrt{2}$.

The wavefront deformation will be seen through shifting/modulation of interferogram spots as shown, for instance, in Fig. 6 (the optical aberrations have been voluntarily amplified in order to show their influence on the interferogram clearly). Then, a reconstruction algorithm will use the information contained in the interferogram to retrieve the input wavefront.

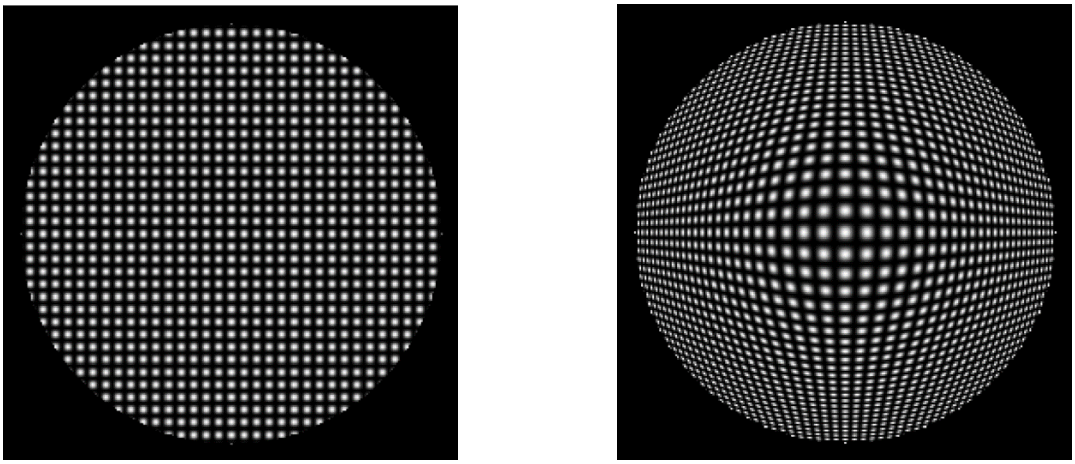

(a) Interferogram obtained with a plane wave.

(b) Interferogram obtained with a large spherical aberration.

Figure 6: Examples of Interferograms generated by the interference of four replicas for different input wavefronts.

3.2 Wavefront Measurement

The optical characterization principle is shown in Fig. 7a. A narrow-band (FWHM = 500 nm) filter at 3.75 µm is used and placed upstream of the spot scan objective. The wavefront analyzer is installed at the same place as the FPA inside the MIRCOS bench. It consists of two elements separated by 4 mm, namely the MHM with a 240 µm period and a 30 µm pitch 320×256 pixel HgCdTe FPA. The wavefront analyzer is placed downstream of the focal plane of the objective, typically at 9 mm in order to ensure that the interferogram covers the whole surface of the FPA as shown in Fig. 7b. The measurement does not require a scan from the spot scan objective, so the interferogram is acquired at a unique objective position.

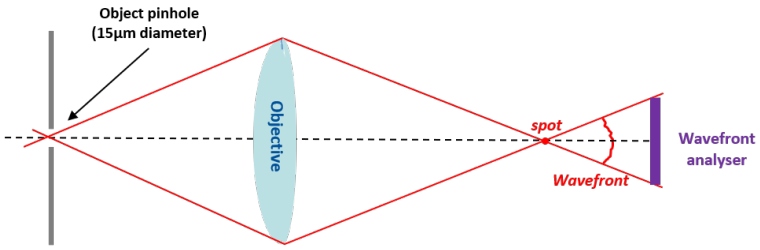

(a) Optical Characterization Principle.

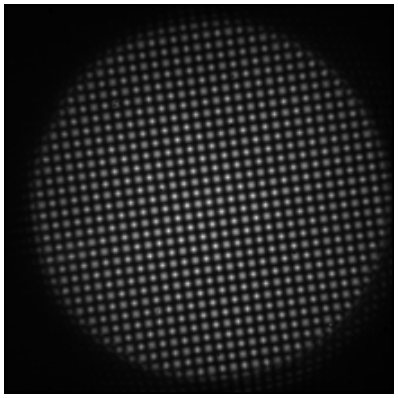

(b) Interferogram obtained after measurement. The image pupil covers the whole surface of the FPA.

Figure 7: Measurement principle.

As explained in Sec. 3.1, an algorithm processes the information in the interferogram and reconstructs the wavefront. The result obtained is shown in Fig. 8.

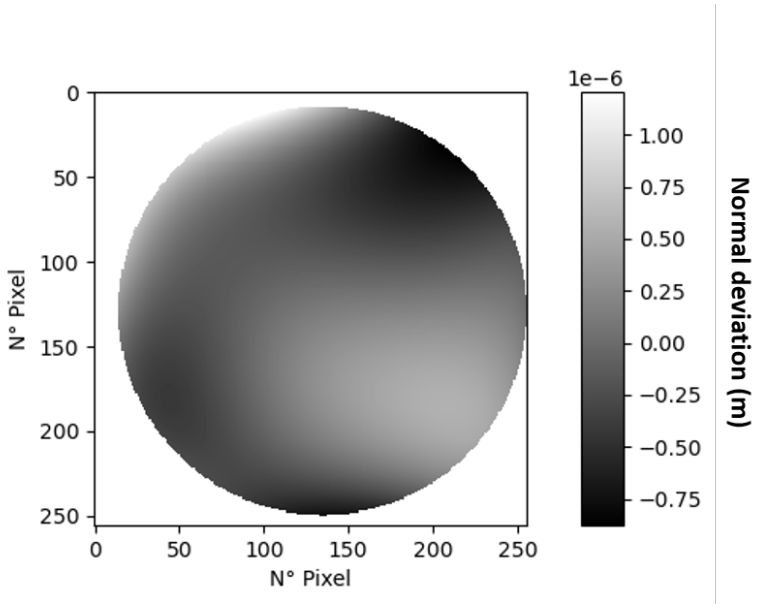

Figure 8: Wavefront reconstruction.

Firstly, as the object pinhole must be perfectly centered with the objective, the primary expected optical aberration is the spherical aberration. However, Fig. 8 does not show the spherical aberration. Moreover, it indicates that the peak-to-valley value of the reconstructed wavefront is about 2 µm, which means that for a wavelength of 3.75 µm (the working wavelength), the peak-to-valley value is approximately about $\lambda/2$. The peak-to-valley strongly depends on values from the edge of the support.

The wavefront shape and the high peak-to-valley value can be explained by the fact that the cooling of the objective is not uniform. Indeed, the cooling of the objective is operated at one contact point by a copper braid, as shown in Fig. 9. This only contact point may cause mechanical constraints on the objective due to the thermal gradient on the objective. Those constraints have a strong influence on the wavefront shape. A possible

improvement to make the cooling more uniform would be to wrap the copper braid around the objective to enable radial cooling. This improvement will allow using the objective optimally and thus provide better optical quality than currently measured.

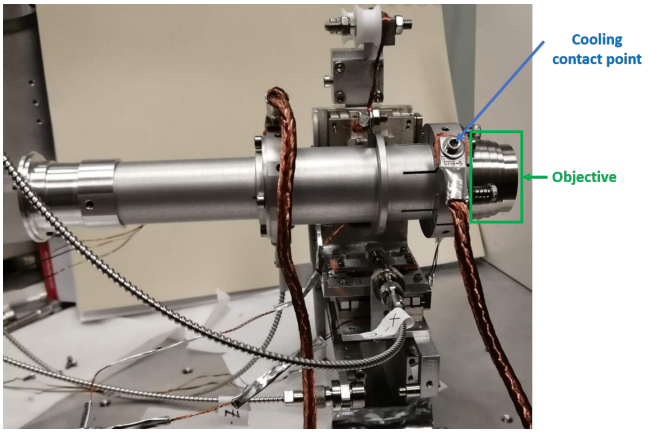

Figure 9: The spot scan objective location and the copper braid contact.

Conclusion

The MIRCOS bench is a versatile cryogenic platform that aims at characterizing small pixels at most 15 µm pitch. The cryogenic spot scan bench allows to scan the FPA with the light spot coming from the objective with a precision of 100 nm. This accuracy is possible thanks to the addition of interferometric sensors enabling an optical control of the linear stages and the mounting of the FPA (to be characterized) directly on the cold shield of the MIRCOS bench.

The first characterization of the wavefront at the output of the objective showed the presence of local defects probably related to a non-uniformity of cooling of the objective.

Improvements are in progress to enhance the uniformity of the cooling. New measurements are planned to validate the new assembly and extract the optimized optical PSF. Spot scan measurements will then be performed on different FPAs of interest for LabEx FOCUS.

Acknowledgment

This work is supported by the LabEx FOCUS (FOCal Plane array for Universe Sensing) gathering nine major laboratories that bring their expertise in the detection field to contribute to the development of better detectors for astronomy and earth observation. This project was partially funded by the DGA (Direction Générale de l'Armement), the ANR (Agence nationale de recherche) via the LabEx FOCUS (ANR-11-LBX-0013) and the "Conseil Général de l'Essonne" (A.S.T.R.E. program).

REFERENCES

[1] Castelein, P., Marion, F., Martin, J.-L., Baylet, J., Moussy, N., Gravrand, O., Durand, A., Chamonal, J.-P., and Destefanis, G., "Megapixel HgCdTe MWIR focal plane array with a 15-um pitch," in [*Detectors and Associated Signal Processing*], **5251**, 65–72, SPIE (Feb. 2004).

[2] Strong, R. L., Kinch, M. A., and Armstrong, J. M., "Performance of 12-µm- to 15-µm-Pitch MWIR and LWIR HgCdTe FPAs at Elevated Temperatures," *Journal of Electronic Materials* **42**, 3103–3107 (Nov. 2013).

[3] Gravrand, O., Destefanis, G., Bisotto, S., Baier, N., Rothman, J., Mollard, L., Brellier, D., Rubaldo, L., Kerlain, A., Destefanis, V., and Vuillermet, M., "Issues in HgCdTe Research and Expected Progress in Infrared Detector Fabrication," *Journal of Electronic Materials* **42**, 3349–3358 (Nov. 2013).

[4] Shkedy, L., Armon, E., Avnon, E., Ari, N. B., Brumer, M., Jakobson, C., Klipstein, P. C., Lury, Y., Magen, O., Milgrom, B., Rosenstock, T., Shiloah, N., and Shtrichman, I., "HOT MWIR detector with 5 um pitch," in [*Infrared Technology and Applications XLVII*], **11741**, 146–157, SPIE (Apr. 2021).

[5] Huang, E., Thomas, J., Hibberd, D., Luong, V., Lott, R., Oleson, M., Hood, A., and MacDougal, M. H., "Small pixel MWIR sensors for low SWaP applications," in [*Infrared Technology and Applications XLVII*], **11741**, 123–129, SPIE (Apr. 2021).

[6] Berthoz, J., Grille, R., Rubaldo, L., Gravrand, O., Kerlain, A., Péré-Laperne, N., Martineau, L., Chabuel, F., and Leclercq, D., "Modeling and Characterization of MTF and Spectral Response at Small Pitch on Mercury Cadmium Telluride," *Journal of Elec Materi* **44**, 1–6 (Sept. 2015).

[7] Shtrichman, I., Fishman, T., Mizrahi, U., Nahum, V., Calahorra, Z., and Aron, Y., "Spatial resolution of SCD's InSb 2D detector arrays," 65423M (Apr. 2007).

[8] Plazas, A. A., Shapiro, C., Smith, R., Huff, E., and Rhodes, J., "Laboratory Measurement of the Brighter-fatter Effect in an H2RG Infrared Detector," *PASP* **130**, 065004 (June 2018).

[9] Primot, J. and Guérineau, N., "Extended Hartmann test based on the pseudoguiding property of a Hartmann mask completed by a phase chessboard," *Appl. Opt., AO* **39**, 5715–5720 (Nov. 2000). Publisher: Optica Publishing Group.

[10] Velghe, S., Primot, J., Guerineau, N., Haidar, R., Cohen, M., and Wattellier, B., "Accurate and highly resolving quadri-wave lateral shearing interferometer, from visible to IR," *Proceedings of SPIE - The International Society for Optical Engineering* **5776** (Feb. 2005).

[11] Velghe, S., Primot, J., Guerineau, N., Ha"idara, R., Demoustierb, S., Cohenc, M., and Wattellier, B., "Advanced wave-front sensing by quadri-wave lateral shearing interferometry - art. no. 62920E," **6292**, 62920E–1 (Aug. 2006).

[12] Velghe, S., Primot, J., Guérineau, N., Cohen, M., and Wattellier, B., "Wave-front reconstruction from multidirectional phase derivatives generated by multilateral shearing interferometers," *Opt. Lett.* **30**, 245 (Feb. 2005).

[13] Velghe, S., *Les nouvelles dimensions de l'interférométrie à décalage quadri-latéral.*, PhD thesis, Université Paris XI (2007).